New Journal of Physics
The open access journal at the forefront of physics

Deutsche Physikalische Gesellschaft DPG
IOP Institute of Physics

Published in partnership with: Deutsche Physikalische Gesellschaft and the Institute of Physics

OPEN ACCESS

RECEIVED
16 July 2015

REVISED
15 October 2015

ACCEPTED FOR PUBLICATION
19 October 2015

PUBLISHED
9 November 2015

PAPER

Quantum enhancement of spin drag in a Bose gas

S B Koller[1,3], A Groot[1], P C Bons[1], R A Duine[2], H T C Stoof[2] and P van der Straten[1]

[1] Nanophotonics, Debye Institute, Center for Extreme Matter and Emergent Phenomena, Utrecht University, PO Box 80,000, 3508 TA Utrecht, The Netherlands
[2] Institute for Theoretical Physics, Center for Extreme Matter and Emergent Phenomena, Utrecht University, PO Box 80,000, 3508 TA Utrecht, The Netherlands
[3] Present address: Physikalisch-Technische Bundesanstalt, Braunschweig, Germany

E-mail: p.vanderstraten@uu.nl

Keywords: ultracold gases, hydrodynamics, spin transport

Abstract

In spintronics the active control and manipulation of spin currents is studied in solid-state systems. Opposed to charge currents, spin currents are strongly damped due to collisions between different spin carriers in addition to relaxation due to impurities and lattice vibrations. The phenomenon of relaxation of spin currents is called spin drag. Here we study spin drag in ultra-cold bosonic atoms deep in the hydrodynamic regime and show that spin drag is the dominant damping mechanism for spin currents in this system. By increasing the phase space density we find that spin drag is enhanced in the quantum regime by more than a factor of two due to Bose stimulation, which is in agreement with recent theoretical predictions and, surprisingly, already occurs considerably above the phase transition.

1. Introduction

The field of spintronics [1–5], where the spin of the electron is manipulated rather than its charge, has recently led to interest in spin currents. Contrary to charge currents, these spin currents can be subject to strong relaxation due to collisions between different spin species, a phenomenon known as spin drag [6]. This effect has been observed for electrons in semi-conductors [7] and for cold fermionic atoms [8–10], where in both cases it is reduced at low temperatures due to the fermionic nature of the particles. We here show that for bosons the opposite behavior occurs and the spin drag is quantum enhanced. This enhancement is due to Bose statistics and gives rise to an extra factor $(1 + n_i)$ for scattering of bosonic particles into states already containing n_i particles. Equivalently, it may be thought of as arising from matching the scattering wave function of two bosonic particles in the gas to the properly symmetrized many-body wavefunction. For fermions one would have Pauli blocking and an extra factor $(1 - n_i)$ that implements the Pauli exclusion principle and in that case forbids scattering into a state that is already occupied.

Figure 1(a) shows an elastic collision between two particles with different spin projection. Due to momentum conservation the mass current $\vec{j}_{\mathrm{m}}$ in this process as shown by the horizontal arrow is conserved. However, the spin current $\vec{j}_{\mathrm{s}}$ is pointing downwards before the collision due to the opposite spin of the two particles as shown by the vertical arrow and this current is reversed by the collision. This is the microscopic origin of spin drag. It is important to emphasize that in electronic systems spin-drag effects also exist, but are usually obscured by the effects of impurities and phonons [6, 7], whereas for ultra-cold atoms they are the only effect. Transport of ultra-cold atoms has been studied in optical lattices [11–16] and through mesoscopic channels [17], but in our study we measure bulk properties irrespective of the external potential.

2. Experiment

In our experiment we produce atoms in two spin states and apply a force on one spin state. We measure the relative displacement of the two clouds with different spin as a function of the time that the force is applied, from

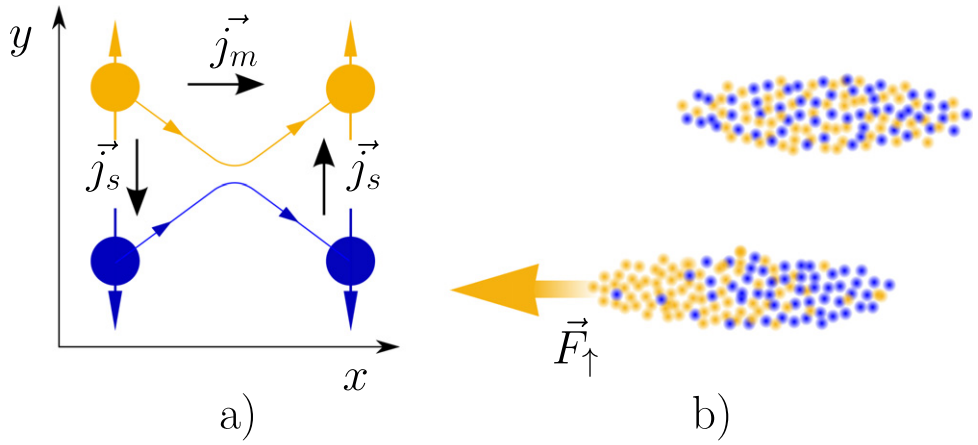

Figure 1. Schematic representation of the experimental method. (a) Velocities of two atoms with different spins in the collision plane before (left side) and after the collision (right side) [7]. Due to the collision the spin current changes sign, which makes it a strong damping mechanism for spin currents. (b) Schematic representation of the measurement: two spin species (*blue*, *yellow*) are prepared and a force acts on only one spin species (*yellow*). Due to the spin drag the other spin species (*blue*) is dragged along.

which we determine the drag rate. We load up to 4.6×10^8 ^{23}Na atoms into a cigar-shaped optical far-off-resonant trap (FORT) with characteristic trap frequencies of $\omega_{\mathrm{rad}}/2\pi = 835$ Hz in the radial and $\omega_{\mathrm{ax}}/2\pi = 3.5$ Hz in the axial direction. The trap is tight in the radial direction to obtain a large density, thereby producing a collisionally opaque and hydrodynamic sample in the axial direction. The temperature is between 2–8 μK and is always kept above the critical temperature for Bose–Einstein condensation. The atoms in the trap are initially all in one spin state, namely the $|F = 1,\ m = -1\rangle$ state (pseudo-spin *up*). The atoms in the $|F = 1,\ m = 0\rangle$ state (pseudo-spin *down*) are produced with a radio-frequency sweep from below the resonance with the magnetic field: 2.6 MHz to 2.71 MHz in 30 to 50 ms. For stability and to maximize the interspecies collisions 50% of the atoms are flipped to the other spin state, creating an equal incoherent mixture of the two spin species. The fraction of atoms in the $|F = 1,\ m = +1\rangle$ state is estimated to be less than 10% and the same for all measurements and does not influence the drag rate within one percent.

We set atoms in one spin state into motion with respect to atoms in the other spin state and observe how the latter are dragged along with the former. The force on the atoms is applied using a magnetic field gradient, which only acts on the spin *up* atoms with $m = -1$ as shown in figure 1(b). The force for the spin *down* atoms with $m = 0$ is zero. After a short period a spin current $\vec{j}_s$ develops:

$$\vec{j}_s = n\Delta\vec{v} = \frac{\vec{F}}{\rho_s}, \tag{1}$$

with n the density, $\Delta\vec{v}$ is the drift velocity difference, and ρ_s the spin resistivity. This relation is identical to Ohm's law for charge currents, but applies here to spin currents. In absence of impurities and an ionic lattice the spin resistivity $\rho_s \equiv m\gamma/n$ is for ultra-cold atoms completely determined by the spin-drag rate γ. The ratio of the applied force F and Δv is proportional to γ.

2.1. Drag method

In figure 2 the force is applied on one spin species such that this cloud is accelerated to the left and due to spin drag the other spin species is dragged along and a relative displacement arises. After the force is switched off, the clouds are cooled in the radial direction by ramping the FORT down in 2 ms and the two spin states are separated by a Stern–Gerlach technique [18] in the radial direction with 5–10 ms time of flight and imaged with absorption imaging. The cooling in the radial direction facilitates the separation of the two clouds in the image and has no effect on the drag. In order to reduce noise and improve sensitivity singular-value decomposition is used to construct an optimized background image, which is used to normalize the absorption image. The upper cloud is in the spin *up* state, whereas the lower cloud is in the spin *down* state. The difference in width of the clouds develops during the detection stage. We determine the center of mass of each cloud by fitting a skewed Gaussian distribution as shown in figure 2(b). The skew in the two distributions is a direct result of the drag of the upper cloud exerted on the lower cloud. Notice that the horizontal separation between the two clouds is small compared to the width of the clouds.

To obtain the spin-drag rate this measurement is repeated for different magnitudes of the force and for different durations during which the force is applied. The result for the relative displacement as a function of

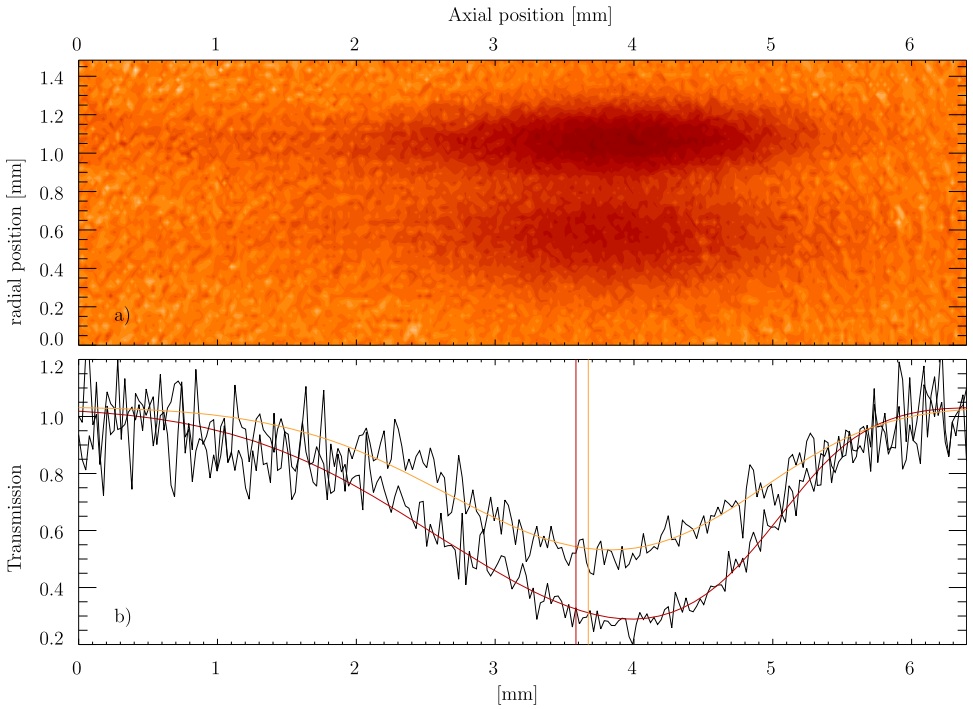

Figure 2. Measurement for the spin drag. A single measurement on a cloud with 1.5×10^8 atoms at 4 μK. The spin species *up* is accelerated with 1.01 m s^{-2} to the left. (a) Pseudo color image of the measured absorption along a line-of-sight through the two clouds. (b) Absorption of the two clouds as a function of the axial position, where the lower curve is for the upper cloud and the upper curve is for the lower cloud. The two curves are obtained by making a line profile through the 2D-image of figure 2(a) at the height of the respective clouds, where the solid lines are fits using skewed Gaussian distributions. The vertical lines indicate the center of mass for the different clouds along the axial direction.

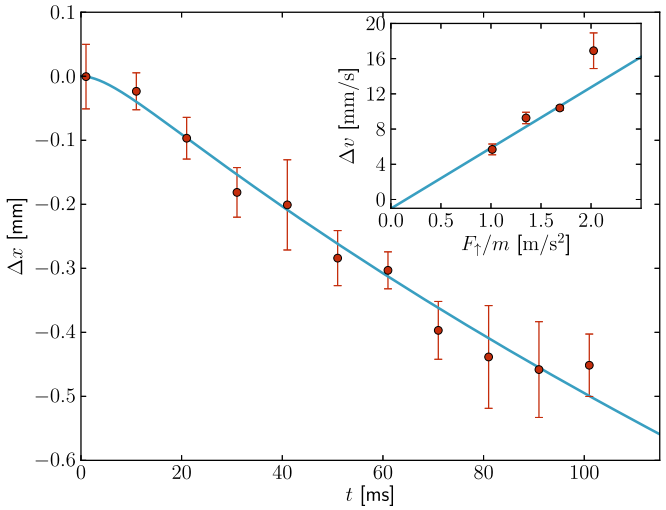

Figure 3. Experimental results for spin drag. Relative displacement Δx between the position of the two clouds as a function of duration t that the force is applied. The data points are indicated by the red dots and the blue line is a fit to the data using the solution of the coupled equations of motion of the two clouds [19]. The inset shows the drift velocity Δv as a function of the strength of the force F. The slope is $(6.9 \pm 1.7) \times 10^{-3}$ s^{-1} and the offset is (-1.0 ± 2.7) mm s^{-1}. All data points are corrected for an offset due to an artifact in the Stern–Gerlach technique, which shifts the axial position of the two clouds with respect to each other by a constant amount. Error bars indicate statistical uncertainties deduced from repeated measurements.

duration t is shown in figure 3. After a short time ($t > 5$ ms) the difference in position between the two clouds is linear in time, indicating that there is a constant drift velocity Δv between the two spin species. In the absence of drag the difference in position will show a quadratic dependence on time due to the ballistic motion of the atoms. The curvature of the fit for short times ($t < 5$ ms) in figure 3 is due to the fact that the two clouds are initially not in a steady state. However, the clouds are collisionally opaque, *i.e.*, they are in the hydrodynamic

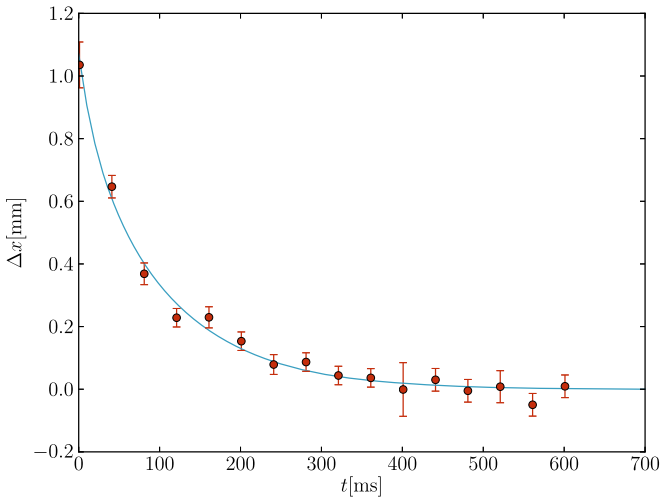

Figure 4. Experimental results for the oscillation method. The relative displacement Δx in position between the two clouds as a function of time t after the release of the atoms. The relative oscillation is overdamped, in which case the decay rate β of the oscillation is given by $\beta = 2\omega_{ax}/\gamma$ with ω_{ax} the oscillation frequency in the trap and γ the drag rate. The red points are the data points and the blue curve is a fit to the data assuming exponential decay.

regime, and the two clouds reach quickly a steady state. In our analysis we allow for this by solving the coupled equations of motion for the centers of the two clouds with only one free parameter [19] and the results are used to extract γ from the data.

Equation (1) is only valid for small applied force F, such that the response of the clouds is still in the linear regime. In [19] it is shown that for ultra-cold atoms to be in the linear-response regime Δv should be well below the thermal velocity $v_{th} = \sqrt{8k_B T/\pi m}$, where k_B is the Boltzmann constant and T the temperature. In the experiments v_{th} is about 6 cm s^{-1}, whereas typical values for Δv are of the order of 1 cm s^{-1}. Thus we expect that our experiments are in the linear regime. In the inset of figure 3 we have tested this assumption by measuring Δv as a function of the acceleration F/m. The straight line is a linear fit to the data with an offset from the origin, which is zero within its uncertainty. This indicates that the measurement is indeed in the linear-response regime for the drag, where equation (1) holds. Since we conducted this measurement with the lowest number of particles and thus lowest drag rate, it follows that all our measurements are in the linear-response regime.

2.2. Oscillation method

The drag method is well suited for large drag rates, but for weak drag a steady state may not be achieved before the two clouds are spatially separated. Therefore for small drag rates we apply the oscillation method. In this method the centers of mass of the two spin species are first separated from each other and then oscillate in the trap. The decay time of the relative oscillation is proportional to the drag rate. In this case, only 3–7 $\times$ 10^6 atoms are loaded into the FORT. Atoms in one spin state are spatially separated from atoms in the other spin state by exerting a constant force on one spin species for a period, after which the force is switched off. The atoms in this spin state start to oscillate in the trap and drag along the atoms in the other spin state, which are initially at rest.

In the oscillation method the separation between the clouds is induced using the same magnetic field as in the drag method and the displacement is well within the range where the FORT is harmonic. Since the drag rate γ is much larger than the axial trap frequency ω_{ax}, the relative oscillation is overdamped and the decay rate is given by

$$\beta = \frac{2{\omega_{ax}}^2}{\gamma}, \tag{2}$$

which allows us to extract the spin-drag rate γ from the measurements (see figure 4). Even for the lowest drag rates the oscillation remains overdamped.

2.3. Analysis of the images

To determine the temperature and number of atoms of the cloud, the absorption images of non-perturbed clouds, which are also not cooled in the radial direction, are analyzed by fitting the column density to the density profile of the ultra-cold atoms. We use the Hartree–Fock theory, where the density profile is determined using only two free parameters, namely the chemical potential μ and the temperature T. In the analysis the trapping frequencies of dipole trap are used, which are obtained by studying the dipole modes of the cloud in the trap in

both the radial and axial direction. The trapping potential is fully determined by the shape of the Gaussian laser beam, which has been measured using a beam profiler. The analysis is more complicated due to the anharmonicity of the trap, but this has been accounted for by using the actual trapping potential in the analysis. The use of the Hartree–Fock theory allows us to determine the fugacity including the effects of interactions on the density profile and the uncertainties in the fugacity has been indicated in the graphs. The uncertainties are mainly determined by the uncertainty in the magnification (1.7%) and the uncertainty in the absorption (10%).

Since the density profile depends only weakly on the fugacity z, we have used an iterative procedure, where first the column density is fitted using a small fugacity ($z = 0.01$) and μ and T are extracted from the fit. Subsequently z is calculated using these two parameters and the fit is repeated using the new value of z. We found that within three iterations the value of μ and T converge within 1%. One benchmark in the determination of z is the appearance of a condensate in the cloud, once the fugacity becomes equal to one. Since the density in the condensate is much larger than in the thermal cloud, it can easily be detected even just below T_c. Furthermore, the value of T_c depends strongly on the number of atoms in a given potential and since we observe T_c at the same temperature in the experiment as expected, this indicates that our determination of the number of atoms, the measured temperature and the shape of our potential is accurate. As a further check the absorption technique is compared in our experiment with the results of the well-established phase-contrast imaging technique [20] and this yields good agreement (within 10%) between the two techniques.

For the data points clouds of atoms are produced using a well-defined evaporative cooling ramp for a selected temperature. We have chosen to analyze unperturbed clouds for μ and T, since in a few cases (low hydrodynamicity) the distributions have been weakly perturbed in the tails due to the drag. This is to be expected, since in the tail the densities are lower and thus also the drag. During the drag measurements several images are acquired of unperturbed clouds to verify that during one drag series the number of atoms or temperature did not change appreciable.

Since the drag velocities ($\approx$1 cm s^{-1}) are smaller than the thermal velocities (6 cm s^{-1}), the temperature of the perturbed clouds did not change significantly due to the drag. The systematic error in the temperature measurement due to the trap anharmonicity has been analyzed using simulations and is caused by the fact that the density distribution is not Gaussian. However, in the current setup this causes only a small systematic shift of the temperature, which remains within the experimental uncertainty.

3. Results

Spin drag is caused by collisions between atoms in different spin states. It is therefore to be expected that the drag rate γ for a classical gas, i.e. in the non-degenerate regime, should be proportional to the interspecies collision rate $\gamma_{\rm col}$ and Vichi and Stringari [21] find $\gamma = (2/3)\gamma_{\rm col}$. The factor $2/3 < 1$, independent of temperature and the density distribution, reflects the fact that for the drag not all collisions contribute equally because only the velocity component in the direction of the force is relevant. For larger phase-space densities the gas can no longer be considered as classical and the effect of quantum statistics becomes important. For our Bose gas collisions are enhanced at low temperatures due to Bose stimulation. This should be contrasted with fermionic systems, where the drag rate is suppressed at low temperatures and goes to zero at $T = 0$ due to Pauli blocking [9, 10]. The scattering process is enhanced due to Bose stimulation to the final states and the enhancement has been determined experimentally as a function of the degeneracy. In this regime we no longer expect to find a temperature-independent proportionality factor between the drag rate and the interspecies collision rate. Therefore, in figure 5 the drag rate is shown as a function of the fugacity $z = \exp(\mu/k_{\rm B}T)$, where μ is the chemical potential of the gas. For $z \ll 1$ the gas is in the classical limit, whereas for $z = 1$ the gas starts to Bose–Einstein condense. Van Driel *et al* [22] showed that the drag rate scaled as γ/T^2 is a function of the fugacity z only.

In figure 5 we plot γ/T^2 as a function of the fugacity z, where z and T are determined from the experiment. For a classical gas γ/T^2 depends linearly on z and the classical result is indicated in the figure with a straight line. Note that this straight line is independent of the density distribution and thus includes the effects of interactions on the density profile. For small z our measurements agree with this result confirming the factor (2/3) between γ and $\gamma_{\rm col}$. For larger values of z the drag rate increases above the classical rate. We evaluated the expression of van Driel *et al* [22] for the drag rate of an inhomogeneous sample using the density distribution of the atoms in our FORT. This requires the trapping potential of the FORT, which is known from the waist and power of the beam. We find the Bose enhancement of the drag rate, as indicated in figure 5 by the blue line. As can be seen from the figure, our results are in good agreement with theory. For large z ($z > 0.5$) the data deviates from the classical model and is in agreement with the quantum model, although the experimental results are slightly larger in this regime compared to the predicted values. These discrepancies can be ascribed to either systematic uncertainties

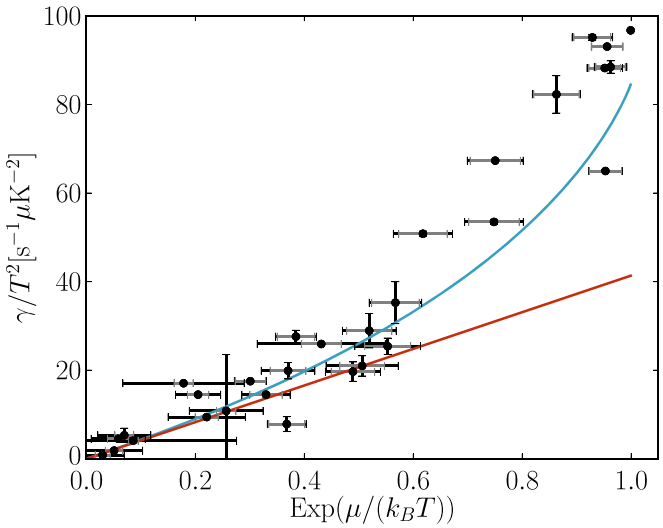

Figure 5. Drag rate versus the fugacity in the degenerate regime. Scaled drag rate γ/T^2 as a function of the fugacity $z = \exp(\mu/k_B T)$. The dots represent the data points, whereas the curves show the results for the spin-drag rate using the classical results of Stringari and Pitaevskii [23] (red curve) and the quantum results of van Driel *et al* [22] (blue curve). Gray bars indicate systematic uncertainties due to magnification and absorption, whereas black bars indicate total uncertainties. Uncertainties in the abscissa are due to uncertainties in the atom number and temperature, whereas uncertainties in the ordinate are due to statistical uncertainties in the drag rate.

in the experiment or by the fact that some assumptions in the theoretical model are not totally fulfilled in the experiment.

As a measure of the accuracy of the theory we use the reduced chi-squared parameter χ^2_{red} [4], which becomes unity for a large number of observations if the data agrees with the theory. For the classical result we obtain $\chi^2_{\mathrm{red}} = 109$, whereas the calculations including Bose enhancement yields $\chi^2_{\mathrm{red}} = 0.45$, showing that the data strongly supports the quantum result over the classical result. We emphasize that here χ^2_{red} is used to compare our experimental results to a theory without any adjustable parameters. Note that the value of χ^2_{red} significantly below one indicates that our error estimates are probably conservative.

For a fully degenerate gas ($z = 1$) the enhancement due to the degeneracy of the gas is more than a factor of two. This is the main result of this letter. The increase of the density due to the degeneracy is taken into account in both the fugacity z and the drag rate γ and thus does not affect the slope of the red curve. Thus the increase of more than a factor of two in the drag rate is solely due to the bosonic stimulation of the scattering process. A similar effect has been observed by Chikkatur *et al* [24] for impurity scattering in a Bose–Einstein condensate. Interestingly this quantum enhancement already becomes detectable for fugacities larger than 0.5 and thus serves as a precursor for the phase transition at $z = 1$.

It is important to realize that the experiments presented here can only be performed when the sample is in the hydrodynamic regime and the relative motion between the two spin clouds is overdamped. In this case the number of collisions during one trap oscillation is much larger than one. To quantify this we can define a hydrodynamicity parameter [25] $\phi = \gamma_{\mathrm{tot}}/\omega_{\mathrm{ax}}$, with γ_{tot} the total collision rate including inter- and intraspecies collisions. For the current experiments we have reached $\gamma_{\mathrm{tot}} = 1400\ \mathrm{s}^{-1}$ at an axial trap frequency of $\omega_{\mathrm{ax}}/2\pi = 3.5$ Hz, yielding a hydrodynamicity of $\phi > 60$. This large hydrodynamicity implies that we are essentially probing bulk properties of the atomic gas and it allows us to quickly reach a steady state. This can for instance be seen in figure 3, where a steady state is reached after 5 ms corresponding to only a few collisions.

4. Conclusion and outlook

In conclusion, we have studied spin drag and determined the spin-drag rate for a gas of ultra-cold bosonic atoms over the entire range of fugacity. We find that in the quantum regime spin drag is Bose enhanced and over a factor of two larger than the classical value, which is in good agreement with a recent theoretical prediction [22]. This shows that the measurement of spin drag is a strong precursor of Bose–Einstein condensation, which, surprisingly, already occurs relatively far above the transition. Our results demonstrate transport properties of

[4] For a non-linear fit with uncertainties in both x- and y-variables we define the reduced chi-squared as $\chi^2_{\mathrm{red}} = \chi^2/(N - m)$ and $\chi^2 = \sum_{i=1}^{N}(y_i - f(x_i))^2/(\Delta y_i{}^2 + (f'(x_i)\Delta x_i)^2)$, where N is the number of measurements and m the degrees of freedom.

ultra-cold bosons in the hydrodynamic regime which are very different from fermionic systems and give a complementary picture of hydrodynamic transport.

Acknowledgments

We would like to thank D van Oosten for stimulating discussions during the experiments, H van Driel and R Kittinaradorn for help with the numerical calculations and R Hulet for critical reading of the manuscript.

References

[1] Wolf S A, Awschalom D D, Buhrman R A, Daughton J M, von Molnr S, Roukes M L, Chtchelkanova A Y and Treger D M 2001 *Science* **294** 1488
[2] Maekawa S and Shinjo T (ed) 2002 *Spin Dependent Transport in Magnetic Nanostructures* (*Advances in Condensed Matter Science*) (Boca Raton, FL: CRC Press)
[3] Žutić I, Fabian J and Sarma S Das 2004 *Rev. Mod. Phys.* **76** 323
[4] Awschalom D D and Flatte M E 2007 *Nat. Phys.* **3** 153
[5] Ohno H 2010 *Nat. Mater.* **9** 952
[6] D'Amico I and Vignale G 2003 *Phys. Rev.* B **68** 045307
[7] Weber C P, Gedik N, Moore J E, Orenstein J, Stephens J and Awschalom D D 2005 *Nature* **437** 1330
[8] Gensemer S D and Jin D S 2001 *Phys. Rev. Lett.* **87** 173201
[9] DeMarco B and Jin D S 2002 *Phys. Rev. Lett.* **88** 040405
[10] Sommer A, Ku M, Roati G and Zwierlein M W 2011 *Nature* **472** 201
[11] Palzer S, Zipkes C, Sias C and Köhl M 2009 *Phys. Rev. Lett.* **103** 150601
[12] Ott H, de Mirandes E, Ferlaino F, Roati G, Modugno G and Inguscio M 2004 *Phys. Rev. Lett.* **92** 160601
[13] Fertig C D, O'Hara K M, Huckans J H, Rolston S L, Phillips W D and Porto J V 2005 *Phys. Rev. Lett.* **94** 120403
[14] Pezzè L, Pitaevskii L, Smerzi A, Stringari S, Modugno G, de Mirandes E, Ferlaino F, Ott H, Roati G and Inguscio M 2004 *Phys. Rev. Lett.* **93** 120401
[15] McKay D, White M, Pasienski M and DeMarco B 2008 *Nature* **453** 76
[16] Henderson K, Kelkar H, Gutiérrez-Medina B, Li T C and Raizen M G 2006 *Phys. Rev. Lett.* **96** 150401
[17] Brantut J-P, Meineke J, Stadler D, Krinner S and Esslinger T 2012 *Science* **337** 1069
[18] Stenger J, Inouye S, Stamper-Kurn D, Miesner H-J, Chikkatur A and Ketterle W 1998 *Nature* **396** 345
[19] Duine R A and Stoof H 2009 *Phys. Rev. Lett.* **103** 170401
[20] Meppelink R, Rozendaal R A, Koller S B, Vogels J M and van der Straten P 2010 *Phys. Rev.* A **81** 053632
[21] Vichi L and Stringari S 1999 *Phys. Rev.* A **60** 4734
[22] van Driel H J, Duine R A and Stoof H T C 2010 *Phys. Rev. Lett.* **105** 155301
[23] Pitaevskii L and Stringari S 2003 *Bose–Einstein Condensation* (Oxford: Oxford University Press)
[24] Chikkatur A P, Görlitz A, Stamper-Kurn D M, Inouye S, Gupta S and Ketterle W 2000 *Phys. Rev. Lett.* **85** 483
[25] Gehm M E, Hemmer S L, O'Hara K M and Thomas J E 2003 *Phys. Rev.* A **68** 011603